

University of Wollongong

Research Online

---

Australian Institute for Innovative Materials -  
Papers

Australian Institute for Innovative Materials

---

1-1-2016

## Manipulating coupling state and magnetism of Mn-doped ZnO nanocrystals by changing the coordination environment of Mn via hydrogen annealing

Yan Cheng  
*Beihang University*

W Li  
*University of Wollongong, wenxian@uow.edu.au*

Weichang Hao  
*Beihang University, whao@buaa.edu.cn*

Huaizhe Xu  
*Beihang University*

Zhongfei Xu  
*University of Wollongong*

*See next page for additional authors*

Follow this and additional works at: <https://ro.uow.edu.au/aiimpapers>

 Part of the [Engineering Commons](#), and the [Physical Sciences and Mathematics Commons](#)

---

### Recommended Citation

Cheng, Yan; Li, W; Hao, Weichang; Xu, Huaizhe; Xu, Zhongfei; Zheng, Li Rong; Zhang, Jing; Dou, S X.; and Wang, Tianmin, "Manipulating coupling state and magnetism of Mn-doped ZnO nanocrystals by changing the coordination environment of Mn via hydrogen annealing" (2016). *Australian Institute for Innovative Materials - Papers*. 1745.

<https://ro.uow.edu.au/aiimpapers/1745>

Research Online is the open access institutional repository for the University of Wollongong. For further information contact the UOW Library: [research-pubs@uow.edu.au](mailto:research-pubs@uow.edu.au)

---

# Manipulating coupling state and magnetism of Mn-doped ZnO nanocrystals by changing the coordination environment of Mn via hydrogen annealing

## Abstract

Mn-doped ZnO nanocrystals are synthesized by a wet chemical route and treated in H<sub>2</sub>/Ar atmosphere with different H<sub>2</sub>/Ar ratios. It is found that hydrogen annealing could change the coordination environment of Mn in ZnO lattice and manipulate the magnetic properties of Mn-doped ZnO. Mn ions initially enter into interstitial sites and a Mn<sup>3+</sup>O<sub>6</sub> octahedral coordination is produced in the prepared Mn-doped ZnO sample, in which the nearest neighbor Mn<sup>3+</sup> and O<sub>2</sub> ions could form a Mn<sup>3+</sup>-O<sub>2</sub>-Mn<sup>3+</sup> complex. After H<sub>2</sub> annealing, interstitial Mn ions can substitute for Zn to generate the Mn<sup>2+</sup>O<sub>4</sub> tetrahedral coordination in the nanocrystals, in which neighboring Mn<sup>2+</sup> ions and H atoms could form a Mn<sup>2+</sup>-O<sub>2</sub>-Mn<sup>2+</sup> complex and Mn-H-Mn bridge structure. The magnetic measurement of the as-prepared sample shows room temperature paramagnetic behavior due to the Mn<sup>3+</sup>-O<sub>2</sub>-Mn<sup>3+</sup> complex, while the annealed samples exhibit their ferromagnetism, which originates from the Mn-H-Mn bridge structure and the Mn-Mn exchange interaction in the Mn<sup>2+</sup>-O<sub>2</sub>-Mn<sup>2+</sup> complex.

## Keywords

hydrogen, via, environment, coordination, changing, nanocrystals, zno, doped, mn, manipulating, state, coupling, annealing, magnetism

## Disciplines

Engineering | Physical Sciences and Mathematics

## Publication Details

Cheng, Y., Li, W., Hao, W., Xu, H., Xu, Z., Zheng, L. Rong., Zhang, J., Dou, S. & Wang, T. (2016). Manipulating coupling state and magnetism of Mn-doped ZnO nanocrystals by changing the coordination environment of Mn via hydrogen annealing. *Chinese physics B*, 25 (1), 017301-1-017301-8.

## Authors

Yan Cheng, W Li, Weichang Hao, Huaizhe Xu, Zhongfei Xu, Li Rong Zheng, Jing Zhang, S X. Dou, and Tianmin Wang

## Manipulating coupling state and magnetism of Mn-doped ZnO nanocrystals by changing the coordination environment of Mn via hydrogen annealing

This content has been downloaded from IOPscience. Please scroll down to see the full text.

2016 Chinese Phys. B 25 017301

(<http://iopscience.iop.org/1674-1056/25/1/017301>)

View [the table of contents for this issue](#), or go to the [journal homepage](#) for more

Download details:

IP Address: 130.130.37.84

This content was downloaded on 15/02/2016 at 04:26

Please note that [terms and conditions apply](#).

# Manipulating coupling state and magnetism of Mn-doped ZnO nanocrystals by changing the coordination environment of Mn via hydrogen annealing\*

Yan Cheng(程岩)<sup>1</sup>, Wen-Xian Li(李文献)<sup>2,3</sup>, Wei-Chang Hao(郝维昌)<sup>1,†</sup>, Huai-Zhe Xu(许怀哲)<sup>1,‡</sup>,  
Zhong-Fei Xu(徐忠菲)<sup>1</sup>, Li-Rong Zheng(郑离荣)<sup>4</sup>, Jing Zhang(张静)<sup>4</sup>,  
Shi-Xue Dou(窦士学)<sup>3</sup>, and Tian-Min Wang(王天民)<sup>1</sup>

<sup>1</sup>Department of Physics and Center of Materials Physics and Chemistry, Beihang University, Beijing 100191, China

<sup>2</sup>Solar Energy Technologies, School of Computing, Engineering and Mathematics, University of Western Sydney, Penrith, NSW 2751, Australia

<sup>3</sup>Institute for Superconducting and Electronic Materials (ISEM), University of Wollongong, Wollongong, NSW 2522, Australia

<sup>4</sup>Beijing Synchrotron Radiation Facility, Institute of High Energy Physics, Chinese Academy of Sciences, Beijing 100049, China

(Received 5 May 2015; revised manuscript received 21 August 2015; published online 30 November 2015)

Mn-doped ZnO nanocrystals are synthesized by a wet chemical route and treated in H<sub>2</sub>/Ar atmosphere with different H<sub>2</sub>/Ar ratios. It is found that hydrogen annealing could change the coordination environment of Mn in ZnO lattice and manipulate the magnetic properties of Mn-doped ZnO. Mn ions initially enter into interstitial sites and a Mn<sup>3+</sup>O<sub>6</sub> octahedral coordination is produced in the prepared Mn-doped ZnO sample, in which the nearest neighbor Mn<sup>3+</sup> and O<sup>2-</sup> ions could form a Mn<sup>3+</sup>-O<sup>2-</sup>-Mn<sup>3+</sup> complex. After H<sub>2</sub> annealing, interstitial Mn ions can substitute for Zn to generate the Mn<sup>2+</sup>O<sub>4</sub> tetrahedral coordination in the nanocrystals, in which neighboring Mn<sup>2+</sup> ions and H atoms could form a Mn<sup>2+</sup>-O<sup>2-</sup>-Mn<sup>2+</sup> complex and Mn-H-Mn bridge structure. The magnetic measurement of the as-prepared sample shows room temperature paramagnetic behavior due to the Mn<sup>3+</sup>-O<sup>2-</sup>-Mn<sup>3+</sup> complex, while the annealed samples exhibit their ferromagnetism, which originates from the Mn-H-Mn bridge structure and the Mn-Mn exchange interaction in the Mn<sup>2+</sup>-O<sup>2-</sup>-Mn<sup>2+</sup> complex.

**Keywords:** coordination environment, magnetic coupling, x-ray absorption fine structure

**PACS:** 73.21.-b, 75.50.Pp, 75.75.-c, 78.70.Dm

**DOI:** 10.1088/1674-1056/25/1/017301

## 1. Introduction

Nowadays, semiconductor devices are a great challenge to data processing and storage capacity. Generally, this could be improved by simultaneously manipulating the spin and charge properties of electrons. Diluted magnetic semiconductor (DMS), a promising candidate for spin-polarized-current-injection material,<sup>[1,2]</sup> especially ZnO has recently attracted extensive attention.<sup>[3,4]</sup> Massive theoretical studies have been conducted and predicted that p-type Mn-doped ZnO could present ferromagnetic behavior at room temperature (RT).<sup>[5-7]</sup> Different magnetic properties in Mn-doped ZnO such as ferromagnetic,<sup>[8,9]</sup> paramagnetic,<sup>[10,11]</sup> or antiferromagnetic behavior<sup>[12]</sup> have been observed. Zheng *et al.*<sup>[12]</sup> showed that Mn-doped ZnO tetrapod structures have a Curie temperature  $T_C = 43$  K, which originates from (Zn, Mn) Mn<sub>2</sub>O<sub>4</sub> at the surface. Cheng and Chien<sup>[13]</sup> observed paramagnetic behavior caused by homogeneous distribution of Mn in epitaxial Mn-doped ZnO thin film. Inamdar *et al.*<sup>[14]</sup> found that incorporation of Mn<sup>2+</sup> ions at substitutional sites in perfect crystal produces a higher saturation magnetic moment than in the undoped material. Through the above researches, we can draw a conclusion that the coordination environment of Mn in ZnO

plays a key role in understanding the magnetic mechanism, and there is a fundamental relation between the observed ferromagnetism and substitutional Mn in the ZnO system. It is very important to investigate the coordination environment of Mn in order to clarify the origin of magnetism in the Mn-doped ZnO system.

The oxidation states and the local coordination of the selected atom, even in a diluted context, can be exactly studied by x-ray absorption fine structure spectroscopy (XAFS).<sup>[15]</sup> By analyzing the Mn and Zn *K*-edge XAFS spectra, Céspedes *et al.*<sup>[16]</sup> found that the ferromagnetism in Mn-doped ZnO originated from high-density regions of Mn cations with a MnO<sub>2-δ</sub> distorted environment at non-stoichiometric and highly defective ZnO grain boundaries. Zhang *et al.*<sup>[17]</sup> suggested that the Mn-doped ZnO system exhibited substantial paramagnetic behavior and the strong antiferromagnetism (AFM) demonstrated by the mere occupation of Zn sites with Mn ions, forming spin-antiparallel pairs and inducing a large structural distortion, which was confirmed by the XAFS spectra.

As is well known, hydrogen is inevitably introduced into the ZnO lattice and will form shallow donors. We have ob-

\*Project supported by the National Basic Research Program of China (Grant No. 2013CB934001) and the National Natural Science Foundation of China (Grant Nos. 51072012 and 51272015).

†Corresponding author. E-mail: whao@buaa.edu.cn

‡Corresponding author. E-mail: hzxu@buaa.edu.cn

tained that (Mn, N) co-doping can enhance the solubility of Mn in the ZnO lattice via reducing the donor binding energy of Mn impurity by orbital hybridization between the N-acceptor and Mn-donor.<sup>[18]</sup> We considered that the donor binding energy of the impurity should decrease if hybridization between H-donors and Mn-donors exists. In addition, some theoretical calculations and experimental results indicated that interstitial hydrogen can induce or enhance ferromagnetism in transition metal (TM) ion doped ZnO.<sup>[19–21]</sup> In a hydrogen annealed Mn-doped ZnO system, the magnetic properties are different, and the source of the observed magnetism is still under intense debate. Manivannan *et al.*<sup>[22]</sup> noted that the magnetism of Mn-doped ZnO is unchanged after hydrogenation. Sharma and Varma<sup>[23]</sup> proposed that the RT ferromagnetism in their hydrogenated sample is generated from oxygen vacancies and Zn interstitials. Our previous work<sup>[20]</sup> has stated that there is a great enhancement of ferromagnetism in hydrogen annealed Co-doped ZnO nanocrystal due to the formation of stable structure Co–H–Co. We supposed that similar structures could be observed by annealing Mn-doped ZnO in hydrogen, which may cause ferromagnetic coupling in the nanocrystal.

The aim of this work is to establish the relationship between the magnetic properties and the coordination environment of Mn in the ZnO lattice. In this work, we synthesize Mn-doped ZnO nanocrystals by the wet chemical route and treat them in H<sub>2</sub>/Ar atmosphere. The Mn coordination environment is investigated by XAFS. We demonstrate that hydrogen annealing can manipulate the coordination environment of Mn, thus inducing magnetic property variation in Mn-doped ZnO.

## 2. Experimental section

Mn-doped ZnO nanocrystals were synthesized by the wet chemical route as described previously.<sup>[18]</sup> The precursor salts (zinc acetate and manganese acetate) were dissolved in dimethyl sulfoxide (DMSO) according to the desired stoichiometry. The total metal ion concentration was 0.1 M. Tetramethylammonium hydroxide (TMAH) was dissolved in ethanol, keeping the concentration at 0.55 M. Then, the ethanol solution of TMAH was dropwise added into the metal salt solution with constant stirring at room temperature. After 48 h, the nanocrystals were precipitated by adding ethyl acetate and removed from the supernatant by centrifugation. Finally, the precipitates were annealed at 873 K in air for 3 h in order to remove the precursor. The obtained powders were annealed under H<sub>2</sub>/Ar atmospheres with different ratios of H<sub>2</sub>:Ar at 873 K for 2 h. The ratios of H<sub>2</sub>/Ar were 1:5 and 4:5, respectively. We denote the as-prepared and H<sub>2</sub> annealed samples as ZnMnO, ZnMnO-H1 (1:5), and ZnMnO-H2 (4:5), respectively.

X-ray diffraction (XRD) patterns were collected on a Rigaku Dmax/C x-ray diffractometer using Cu K $\alpha$  radiation

operated at 40 kV and 200 mA. Mn K-edge x-ray absorption near edge structure (XANES) and extended x-ray absorption fine structure (EXAFS) spectra were collected in fluorescence mode due to the lower concentration of Mn on Beamline 1W1B at the Beijing Synchrotron Radiation Facility and Beamline BL14W on the Shanghai Synchrotron Radiation Facility. Raman spectra were collected on an HR800 LabRam Infinity spectrometer excited by a continuous Ar<sup>+</sup> laser with a wavelength of 514 nm. The magnetic measurements were carried out using a physical properties measurement system (PPMS; Quantum Design) equipped with a vibrating sample magnetometer.

## 3. Result and discussion

### 3.1. Characterization of the coordination environment

Figure 1 shows x-ray diffraction (XRD) patterns of ZnMnO, ZnMnO-H1, and ZnMnO-H2. All the diffraction peaks could be attributed to pure ZnO with a wurtzite structure. No secondary phase is detectable within the resolution of XRD. Figure 2 shows the TEM images of ZnMnO and ZnMnO-H2. There is no obvious variation between these two samples, which indicates that annealing under H<sub>2</sub>/Ar atmosphere has no effect on the morphology of ZnMnO.

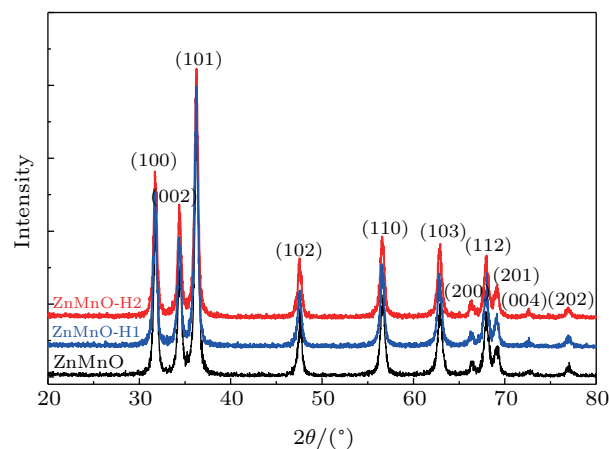


Fig. 1. (color online) XRD patterns of ZnMnO, ZnMnO-H1, and ZnMnO-H2.

Figure 3 shows the normalized Mn K-edge XANES spectra of ZnMnO, ZnMnO-H1, ZnMnO-H2, MnO, Mn<sub>2</sub>O<sub>3</sub>, and ZnO reference samples. For comparison between Zn and Mn XANES spectra, the energy is rescaled to the respective absorption K-edges calculated from the first derivative of the XANES signal.<sup>[24]</sup> The Mn K-edge energy is used to characterize the average Mn oxidation state. The main edge energy shifts toward lower energy from ZnMnO to ZnMnO-H2, indicating a decrease in the oxidation state with increasing the value of H<sub>2</sub>/Ar. The peaks with positions marked by the dotted lines for our samples are the characteristic peaks of MnO and Mn<sub>2</sub>O<sub>3</sub>, which reveal that Mn oxidation states range between Mn<sup>2+</sup> and Mn<sup>3+</sup>. The valence of

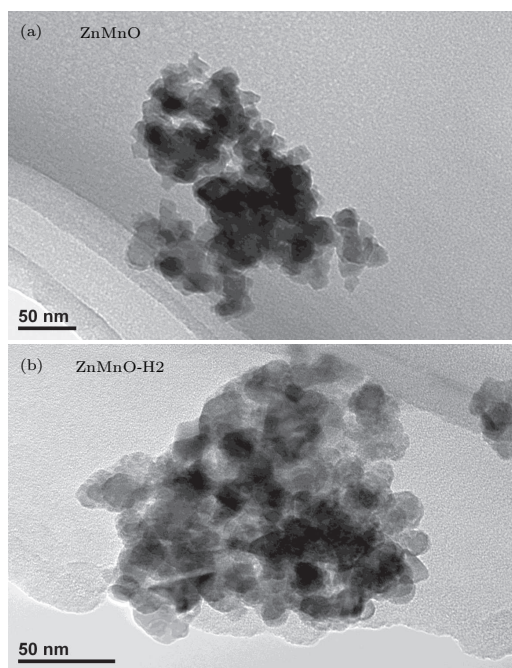


Fig. 2. TEM images of ZnMnO (a) and ZnMnO-H2 (b).

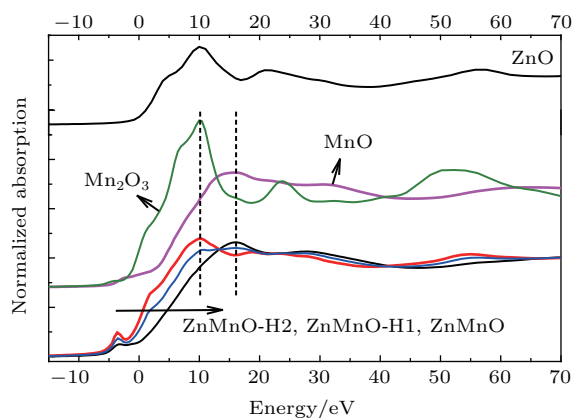


Fig. 3. (color online) Normalized Mn *K*-edge XANES spectra of ZnMnO, ZnMnO-H1, ZnMnO-H2, and the reference samples of MnO, Mn<sub>2</sub>O<sub>3</sub>, and ZnO.

Mn in the un-hydrogenated sample is about +3, and ZnMnO-H2 mainly presents Mn<sup>2+</sup> oxidation states, while in ZnMnO-H1, Mn ions are found to be in a mixed valence state of Mn<sup>2+</sup> and Mn<sup>3+</sup>. Furthermore, the difference between the Mn *K*-edge features of ZnMnO and the Zn *K*-edge features of ZnO at 10–70 eV indicates that the chemical environment of Mn in ZnMnO is different from that of Zn in ZnO. It implies that the Mn<sup>3+</sup> ions do not substitute for Zn in the ZnMnO sample. When annealing in H<sub>2</sub>/Ar, the similar features at about 10–70 eV between the Mn *K*-edge of ZnMnO-H1 and the Zn *K*-edge of ZnO reveal that the chemical environment of some Mn is the same as that of Zn in ZnO. This means that part of the Mn<sup>3+</sup> ions have substituted for Zn<sup>2+</sup> in ZnO. With increasing the value of H<sub>2</sub>/Ar, the features in the post-edge region between the Mn *K*-edge of ZnMnO-H2 and the Zn *K*-edge of ZnO are almost the same, which reveals that most of the Mn ions have substituted for Zn.

Figure 4 shows the Mn *K*-edge Fourier transforms of the  $k^3\chi(k)$  functions of the EXAFS spectra. For comparison, the Mn *K*-edges of MnO, Mn<sub>2</sub>O<sub>3</sub>, and MnOOH, as well as Zn *K*-edge of pure ZnO, are presented along with those of the ZnMnO samples. Here, P<sub>1</sub> (1.41 Å) and P<sub>3</sub> (2.41 Å) are attributed to the first Mn–O and the second Mn–Mn coordination shells of MnO<sub>6</sub> in MnOOH,<sup>[25]</sup> respectively. P<sub>2</sub> (1.55 Å) and P<sub>4</sub> (2.93 Å) respectively represent the first Zn–O and the second Zn–Zn shells in ZnO. The coordination of Mn in Mn-doped ZnO turn into a four Mn–O bonded Mn<sup>2+</sup>O<sub>4</sub> tetrahedron while Mn substitutes for Zn. In ZnMnO nanocrystals, there are two peaks located at 1.41 Å and 2.41 Å, which means that the coordination environment of Mn mainly performs as the MnO<sub>6</sub> octahedral configuration. In the ZnMnO-H2 sample, two peaks at 1.55 Å and 2.93 Å indicate that Mn ions are demanded by MnO<sub>4</sub> tetrahedral configuration. In the ZnMnO-H1 sample, three main coordination peaks are found as shown in Fig. 4. Peak A between peak P<sub>1</sub> and P<sub>2</sub> corresponds to the Mn–O coordination. The other two coexisting peaks, B and C appearing at the positions of P<sub>3</sub> and P<sub>4</sub>, represent the Mn–Mn coordination in MnO<sub>6</sub> and the Mn–Mn(Zn) coordination in MnO<sub>4</sub>, respectively. These illustrate that there are two different configurations of Mn in ZnMnO-H1 nanocrystal. As shown in the inset of Fig. 4, the calculated areas of peaks B and C according to the Gauss fitting are explained as being due to the fact that the content ratio between MnO<sub>4</sub> and MnO<sub>6</sub> in ZnMnO-H1 is about 4:1.

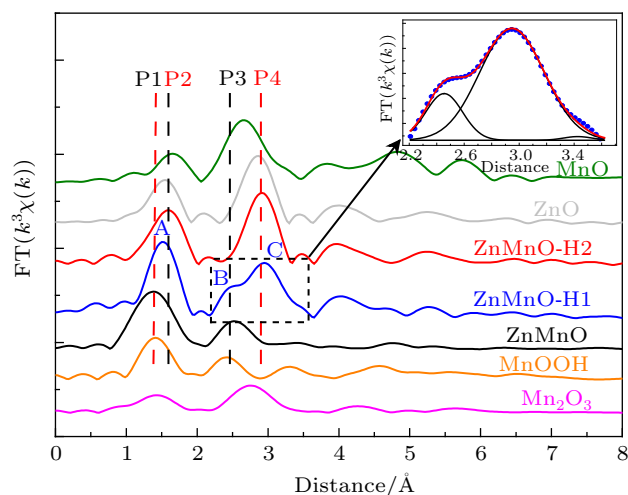


Fig. 4. (color online) Mn *K*-edge Fourier transforms of  $k^3\chi(k)$  functions of EXAFS spectra without phase correction for ZnMnO, ZnMnO-H1, and ZnMnO-H2, together with reference samples MnO, Mn<sub>2</sub>O<sub>3</sub>, MnOOH, and ZnO. The inset shows the Gauss fitting of peaks B and C.

Figure 5 shows the room-temperature Raman spectra of our samples. Compared with the spectrum of pure ZnO that we synthesized, we observe six modes at about 99.4, 332.3, 384.4, 438.6, 484.5, and 579.9 cm<sup>-1</sup> corresponding to E<sub>2</sub><sup>low</sup>, 2-E<sub>2</sub>(M), A<sub>1</sub><sup>TO</sup>, E<sub>2</sub><sup>high</sup>, an interface or surface phonon mode (SPM), and A<sub>1</sub><sup>LO</sup> mode, respectively.<sup>[26]</sup> Two additional modes

at about  $526.9\text{ cm}^{-1}$  and  $665.1\text{ cm}^{-1}$  are denoted as AM1 and AM2. AM1 is assigned to the mode due to  $\text{Mn}^{2+}$  dissolved in the ZnO lattice.<sup>[27,28]</sup> The origin of AM2 is still under intense debate. Samanta *et al.*<sup>[29]</sup> and Cong *et al.*<sup>[30]</sup> attributed it to the second phases  $\text{ZnMn}_2\text{O}_4$  and  $\text{ZnMnO}_3$ , respectively. Yet there are no second phases in our samples. In the literature, this mode is reported in the Raman spectra of  $\text{Mn}_2\text{O}_3$ <sup>[31]</sup> and  $\text{MnOOH}$ .<sup>[32]</sup> As with our samples, the coordination environments of Mn in  $\text{ZnMn}_2\text{O}_4$ ,  $\text{ZnMnO}_3$ ,  $\text{Mn}_2\text{O}_3$ , and  $\text{MnOOH}$  are also in the form of a  $\text{MnO}_6$  octahedron. As a result, we attribute AM2 to a mode arising from  $\text{MnO}_6$  octahedral coordination. As shown in Fig. 5, the decreasing of the intensity of AM2 results from the decreasing of the concentration of  $\text{MnO}_6$  octahedron with increasing the value of  $\text{H}_2:\text{Ar}$ , which is consistent with the EXAFS spectra.

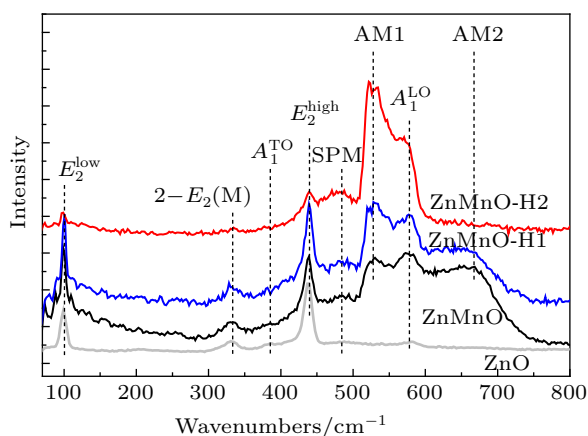


Fig. 5. (color online) Raman spectra of ZnO, ZnMnO, ZnMnO-H1, and ZnMnO-H2.

There are two main positions of Mn in the ZnO lattice after doping. One is interstitial, with the Mn ions forming the  $\text{MnO}_6$  octahedral configuration as shown in Fig. 6(a); the other is Mn substitution for Zn, forming the  $\text{MnO}_4$  tetrahedral configuration (Fig. 6(b)). The different Mn oxidation states and local environments of our samples are shown in Table 1. As mentioned above, the coordination of Mn in the as-prepared ZnMnO is primarily that in  $\text{MnO}_6$ , which means that most Mn ions are in interstitial sites in the ZnO lattice. In ZnMnO-H2, the coordination of most Mn ions are those in  $\text{MnO}_4$ , which is similar to the coordinates of  $\text{ZnO}_4$  in ZnO. This reveals that most Mn ions substitute for Zn ions in the ZnO lattice. From the above analysis, we can conclude that hydrogen annealing can control the coordination environment of Mn in the ZnO lattice, i.e., it changes from  $\text{Mn}^{3+}\text{O}_6$  octahedral coordination to  $\text{Mn}^{2+}\text{O}_4$  tetrahedral coordination. As we discussed octylamine treatment of Mn-doped ZnO,<sup>[18]</sup> the estimated donor binding energy of an impurity ( $E_B$ ) can be expressed as

$$E_B = \frac{e^2}{2\epsilon} \frac{1}{a_d}. \quad (1)$$

Here, the dielectric constant,  $\epsilon$ , and the charge of the electron,  $e$ , are all constant. So  $E_B$  only depends on the value of the Bohr radius of the donor,  $a_d$ . In the as-prepared sample, the donor binding energy of the impurity is induced by  $\text{Mn}^{3+}$ , in which there are four electrons in the d-shell. When the sample is annealed in hydrogen, H can offer an electron to the  $\text{Mn}^{3+}$  ion and form a covalent bond with it. The hybridization between Mn and H would enhance the value of  $a_d$ . According to Eq. (1),  $E_B$  would decrease with increasing the value of  $\text{H}_2:\text{Ar}$ , which induces a transformation of the  $\text{Mn}^{3+}\text{O}_6$  octahedron into  $\text{Mn}^{2+}\text{O}_4$  tetrahedron.

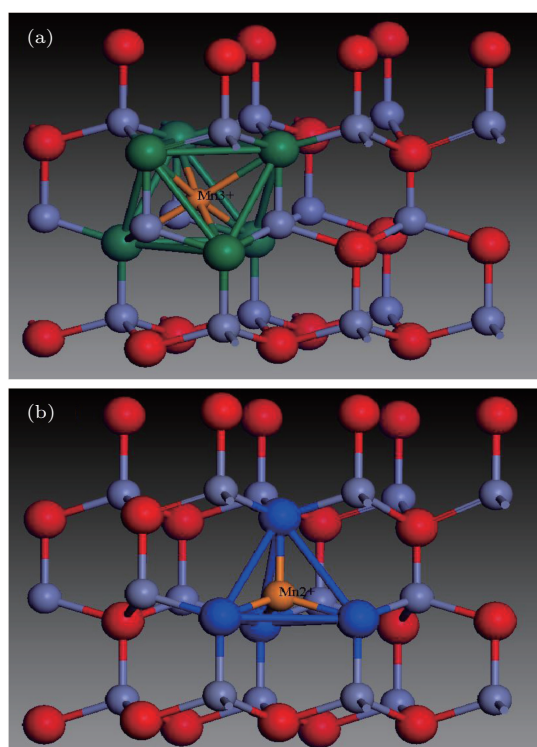


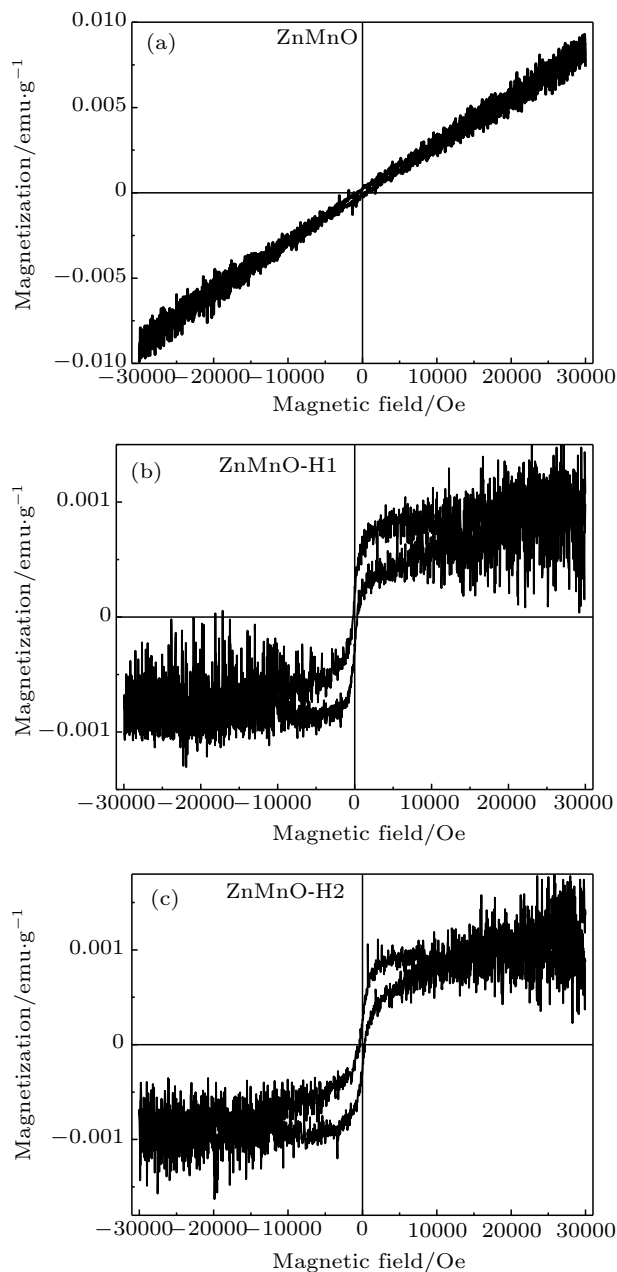
Fig. 6. (color online) Schematic diagrams of the interstitial site (a) and the substitutional site (b) of Mn in the ZnO lattice after doping.

### 3.2. Magnetic properties

Figures 7(a)–7(c) demonstrate the curves of RT magnetization versus field ( $M-H$ ). The as-prepared nanocrystal exhibits RT paramagnetism (PM), while the sample annealed in  $\text{H}_2/\text{Ar}$  atmosphere is ferromagnetic (FM). The values of saturation magnetization ( $M_S$ ) of ZnMnO-H1 and ZnMnO-H2 are 0.008 and 0.01 emu/g, respectively. Our previous work<sup>[33]</sup> shows that the as-prepared Mn-doped ZnO nanocrystal is antiferromagnetic, and the Neel temperature is below RT. As a result, ZnMnO shows PM at RT. In addition, there is a similar variation between  $M_S$  and the content of  $\text{Mn}^{2+}\text{O}_4$  tetrahedron, together with the  $\text{H}_2$  content as shown in Table 1. This results in the fact that RT ferromagnetism is related to the  $\text{Mn}^{2+}\text{O}_4$  tetrahedral coordination and H in a ZnO lattice.

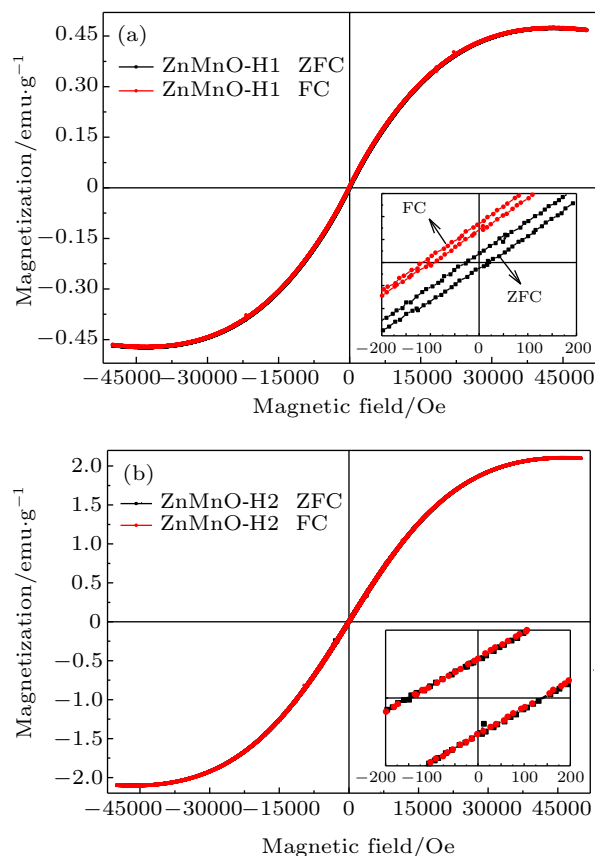
**Table 1.** Valence, main state of Mn in the ZnO lattice, the local coordination of Mn, and RT magnetic property in ZnMnO, ZnMnO-H1, and ZnMnO-H2.

Samples	Valence	State of Mn in ZnO	Local coordination	RT magnetic property
ZnMnO	+3	interstitial	MnO <sub>6</sub>	PM
ZnMnO-H1	+3&+2	interstitial & substitution	MnO <sub>6</sub> & MnO <sub>4</sub>	FM (0.008 emu/g)
ZnMnO-H2	+2	substitution	MnO <sub>4</sub>	FM (0.01 emu/g)

**Fig. 7.** (color online) RT  $M$ - $H$  curves of ZnMnO (a), ZnMnO-H1 (b), ZnMnO-H2 (c).

We also measure  $M$ - $H$  curves of ZnMnO-H1 and ZnMnO-H2 at 5 K after cooling from 350 K in 0 and 1000 Oe fields. The loops of zero-field cooling (ZFC) and field cooling (FC) hysteresis are shown in Figs. 8(a) and 8(b). All the samples are ferromagnetic, and the values of  $M_S$  are 0.472, and 2.104 emu/g, respectively. In the ZnMnO-H1 sample as plotted in the enlargement near the low-field region in Fig. 8(a), the hysteresis loop maintains good central symmetry in the

ZFC process but displays negative exchange bias behavior in the FC, with the exchange bias field being about 70 Oe in the FC process. As is well known, the exchange bias phenomenon is generally ascribed to the exchange coupling at the interface between the ferromagnetic layer and the antiferromagnetic layer.<sup>[34]</sup> It is also reported that there is exchange bias in a single-phase magnet, such as Ru<sub>0.25</sub>Cr<sub>0.75</sub>O,<sup>[35]</sup> YbFe<sub>2</sub>O<sub>4</sub>.<sup>[36]</sup> As a result, the exchange bias behavior observed at 5 K proves that the system must contain at least two exchange-coupled states, such as antiferromagnetic phase and ferromagnetic coupling. The structural results testify that both Mn<sup>3+</sup>O<sub>6</sub> octahedron and Mn<sup>2+</sup>O<sub>4</sub> tetrahedron exist in the ZnMnO-H1 sample. There is no exchange bias phenomenon in ZnMnO-H2 (Fig. 8(b)), in which Mn ions mainly exist in the form of Mn<sup>2+</sup>O<sub>4</sub> tetrahedron. Combining the above results and analysis, we believe that antiferromagnetic coupling is induced by Mn<sup>3+</sup>O<sub>6</sub> octahedral coordination, while ferromagnetic coupling is due to Mn<sup>2+</sup>O<sub>4</sub> tetrahedral coordination and some H-related structures.<sup>[23]</sup>

**Fig. 8.** (color online) ZFC and FC (for 1000 Oe)  $M$ - $H$  curves measured at 5 K for (a) ZnMnO-H1 and (b) ZnMnO-H2. The insets show the enlarged low-field regions of these two samples.



Figures 9(a)–9(c) show the variations of magnetization with temperature ( $M$ – $T$  curve) of ZnMnO, measured in a temperature range from 5 K to 350 K in a magnetic field of 1000 Oe. In order to further investigate the phase transition, we calculate the inverse magnetic susceptibility as a function of temperature ( $1/\chi$ – $T$  curve) from  $M$ – $T$  data. There are magnetic phase transitions at about 100 K in all samples. Martínez *et al.*<sup>[37]</sup> considered it as an AFM–PM phase transition. Linear fitting of the  $1/\chi$ – $T$  curve from 5 K to 250 K is carried out in

these three samples, and the fitting formulas are  $\chi = 0.71/(T + 39.9)$ ,  $\chi = 0.86/(T + 124.5)$ , and  $\chi = 0.9/(T + 34.2)$ , respectively. According to the Curie–Weiss formula,  $\chi = C_0/(T + \theta_0)$ , we can obtain the value of the Curie–Weiss temperature,  $\theta_0$ , and the Curie constant,  $C_0$ , as shown in Table 2. The negative value of  $\theta_0$  verifies the existence of antiferromagnetic coupling in each of our three samples. The antiferromagnetic behavior could be assigned to the magnetic interaction between trivalent Mn ions in  $\text{Mn}^{3+}\text{O}_6$  octahedral coordination. The Curie constant can be given as

$$C_0 = \frac{(g\mu_B)^2 S(S+1)n}{3k_B}, \quad (2)$$

where  $g$  is the Lande factor,  $S$  is the spin quantum number,  $\mu_B$  is the Bohr magneton,  $k_B$  is the Boltzman constant, and  $n$  is the number of cation sites per unit volume. The exchange integral between the nearest neighbors  $J$  can be explained as

$$J = \frac{3k_B\theta_0}{2zS(S+1)}, \quad (3)$$

where  $z$  is the number of nearest-neighbor cations in the case of the wurtzite structure, and  $\theta_0$  is the Curie–Weiss temperature. According to Eqs. (2) and (3),  $J$  can be obtained from

$$J = n \frac{\theta_0 (g\mu_B)^2}{C_0 2z}, \quad (4)$$

where  $(g\mu_B)^2/2z$  is constant. So the value of  $J$  only depends on the value of  $n\theta_0/C_0$ , with  $\theta_0$  and  $C_0$  being evaluated from the extrapolation line, and  $n$  being in direct proportion to the number of  $\text{Mn}^{3+}$ . Table 2 summarizes the values of  $\theta_0$ ,  $C_0$ ,  $n$ , and  $J$ . As the density of  $\text{Mn}^{3+}\text{O}_6$  octahedron decreases, the magnitude of  $J$  decreases. This confirms the strong antiferromagnetic exchange coupling in the as-prepared sample and the weak antiferromagnetic coupling in the hydrogen annealed samples. This calculated result provides further evidence to support our hypothesis that antiferromagnetic coupling originates from the  $\text{Mn}^{3+}\text{O}_6$  octahedron.

There is other magnetic phase transition at about 250 K in both hydrogen annealed samples as displayed in Figs. 9(b) and 9(c). We consider this as an FM–PM transition because the  $1/\chi$ – $T$  curve is similar to the scenario in the schematic diagram of the FM–PM phase transition. Annealing in  $\text{H}_2$  is an effective method to enhance  $M_S$  in  $\text{ZnCoO}$ <sup>[20]</sup> or  $\text{ZnMnO}$ <sup>[23]</sup> nanocrystal. Also, this FM–PM phase transition only appears in the annealed sample but not the as-prepared sample, which makes us propose that the ferromagnetic behavior below 250 K could be attributed to some H-related configurations in the hydrogen annealed samples.

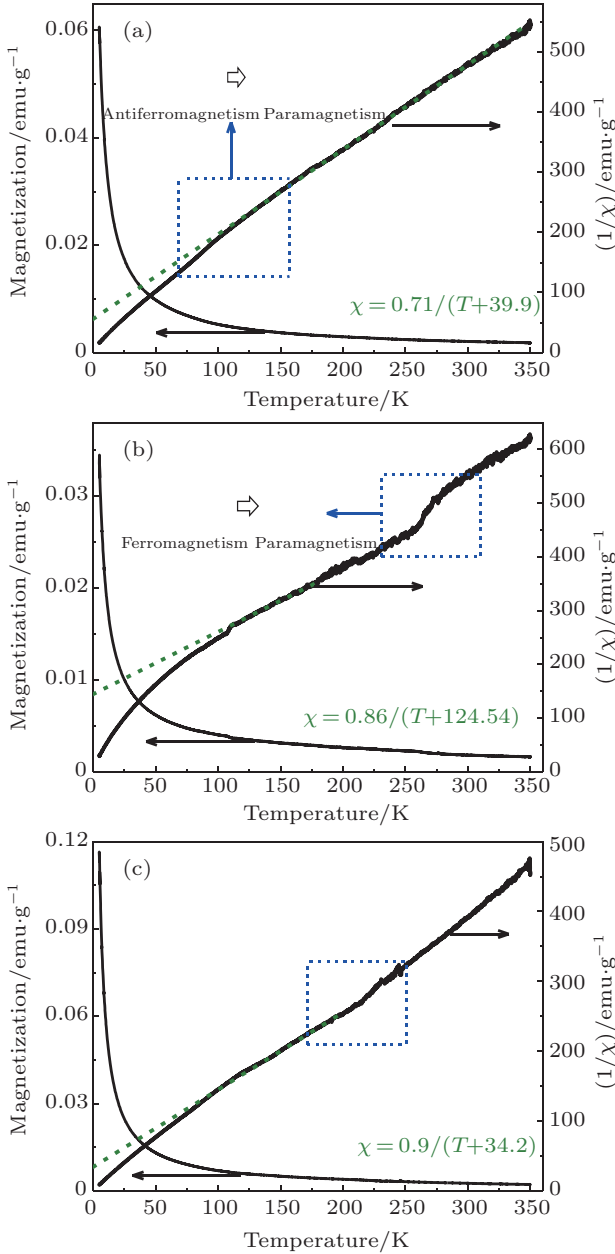


**Fig. 9.** (color online) (a)–(c) The  $M$ – $T$  and  $1/\chi$ – $T$  curves of ZnMnO, ZnMnO-H1, and ZnMnO-H2 in a temperature ranging from 5 to 350 K in a magnetic field of 1000 Oe.

**Table 2.** Values of  $\theta_0$ ,  $C_0$ ,  $\theta_0/C_0$ ,  $n$ , and  $J$ .

Samples	$\theta_0/\text{K}$	$C_0/\text{g}\cdot\text{K}\cdot\text{emu}^{-1}$	$(\theta_0/C_0)/\text{emu}\cdot\text{g}^{-1}$	$n/\text{arb. units}$	$J/\text{arb. units}$
ZnMnO	–39.9	0.71	–56.2	$\sim 1$	$\sim -56$
ZnMnO-H1	–124.5	0.86	–144.8	$\sim 0.2$	$\sim -29$
ZnMnO-H2	–34.2	0.9	–38	$\ll 0.1$	$\ll -3.8$

In order to establish the relationship between the magnetic coupling and the coordination environment of Mn in the ZnO lattice, crystal lattice and energy level diagrams of a  $\text{Mn}^{3+}\text{O}_6$  octahedron at an interstitial site and a  $\text{Mn}^{2+}\text{O}_4$  tetrahedron at a substitutional site are given in Fig. 10. In the as-prepared sample (Fig. 10(a)), the neighboring Mn ions in the  $\text{Mn}^{3+}\text{O}_6$  octahedron form a  $\text{Mn}^{3+}-\text{O}^{2-}-\text{Mn}^{3+}$  complex with a bond angle of  $180^\circ$ . According to the superexchange interaction,<sup>[38]</sup> one p electron of the O atom would couple with the  $e_g$  orbital of  $\text{Mn}^{3+}$ . In addition, this electron in the p orbital of the O atom must be antiparallel to the  $e_g$  orbital, which makes the two neighboring  $\text{Mn}^{3+}$  ions antiparallel. Thus, the system exhibits antiferromagnetic behavior. It also explains why most researchers have observed antiferromagnetic behavior in Mn-dopant ZnO. When the nanocrystal is annealed under  $\text{H}_2$ , many interstitial H ( $\text{H}_i$ ) atoms are incorporated into the nanocrystal. We hold the opinion that the substitutional Mn ( $\text{Mn}^{2+}\text{O}_4$  tetrahedron) and  $\text{H}_i$  would form a Mn–H–Mn bridge structure. A similar structure has been reported by Park *et al.*<sup>[39]</sup> through electron paramagnetic resonance and nuclear

magnetic resonance spectra. In this case, the spins of the two neighboring substitutional Mn ions become parallel via the  $\text{H}_i$  mediator, as shown in Fig. 10(b). This Mn–H–Mn bridge structure leads to the enhancement of ferromagnetic coupling in hydrogen annealed nanocrystals, as we have observed in hydrogen annealed Co-doped ZnO nanocrystals.<sup>[20]</sup> Another reason which gives rise to FM may originate from ferromagnetic coupling to the exchange interaction between two neighboring  $\text{Mn}^{2+}$  ions. In Fig. 10(c), the bond angle of  $\text{Mn}^{2+}-\text{O}^{2-}-\text{Mn}^{2+}$  is  $120^\circ$  and the distance between Mn ions decreases when Mn ions substitute for Zn ions. Consequently, the neighboring  $\text{Mn}^{2+}$  ions can couple with each other and a parallel ferromagnetic coupling is produced between the two neighboring  $\text{Mn}^{2+}$  ions. Our results clearly point out the relationship between the magnetic properties and the coordination environment of Mn in the ZnO lattice. This relationship may provide a new perspective for understanding the current controversial experimental results in transition metal doped DMSs. It should be seriously taken into account in future DMS studies.

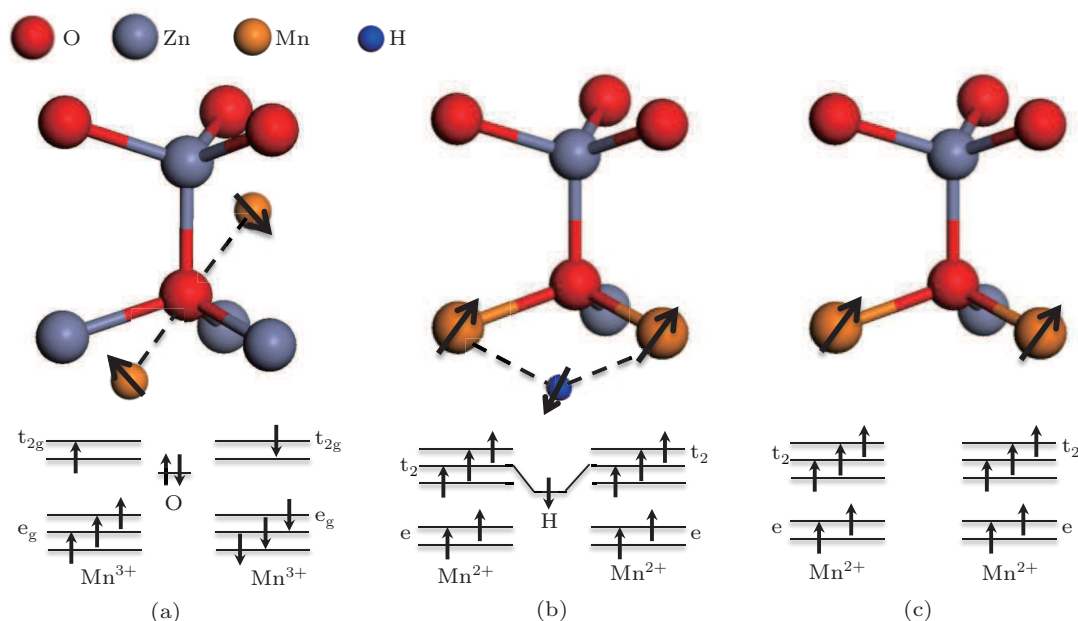


**Fig. 10.** Crystal lattice and energy level diagrams of (a)  $\text{Mn}^{3+}\text{O}_6$  octahedron at interstitial site and  $\text{Mn}^{3+}-\text{O}^{2-}-\text{Mn}^{3+}$  complex, (b)  $\text{Mn}^{2+}\text{O}_4$  tetrahedron at substitutional site and  $\text{Mn}^{2+}-\text{H}-\text{Mn}^{2+}$  complex, (c)  $\text{Mn}^{2+}\text{O}_4$  tetrahedron at substitutional site and  $\text{Mn}^{2+}-\text{Mn}^{2+}$  complex.

#### 4. Conclusions

We synthesize Mn-doped ZnO nanocrystals by a wet chemical route and post hydrogen annealing. Our results indicate that Mn ions initially enter into interstitial sites in the ZnO lattice and form  $\text{Mn}^{3+}\text{O}_6$  groups with an octahedral coordination in the as-prepared sample. Hydrogen annealing can change the state of Mn into  $\text{Mn}^{2+}\text{O}_4$ , which has a tetrahedral coordination at the substitutional sites. Antiferromagnetism of as-prepared nanocrystals, originating from the interactions of the  $\text{Mn}^{3+}-\text{O}^{2-}-\text{Mn}^{3+}$  complex in the octahedral coordina-

tion, is obtained. The annealed sample exhibits ferromagnetic behavior due to the Mn–H–Mn bridge structure and Mn–Mn complex in the tetrahedral coordination. Our results suggest that the coordination environment of Mn can be changed with hydrogen annealing, which generates a significant effect on the magnetic properties of Mn-doped ZnO. The relationship between the magnetic coupling and Mn coordination environment will provide a new perspective for manipulating magnetic coupling mechanism in DMSs.

## Acknowledgment

The authors thank Dr. T. Silver for her useful discussion, and also the teams of Beamline 1W1B at the Beijing Synchrotron Radiation Facility and Beamline BL14W at the Shanghai Synchrotron Radiation Facility for the measurements of Mn *K*-edge EXAFS spectra.

## References

- [1] Pearton S J, Abernathy C R, Norton D P, Hebard A F, Park Y D, Boatner L A and Budai J D 2003 *Mater. Sci. Eng. R* **40** 137
- [2] Akinaga H and Ohno H 2002 *IEEE Trans. Nanotechnol.* **1** 19
- [3] Ohno Y, Young D K, Beschoten B, Matsukura F, Ohno H and Awschalom D D 1999 *Nature* **402** 790
- [4] Ohno H, Chiba D, Matsukura F, Omiya T, Abe E, Dietl T, Ohno Y and Ohtani K 2000 *Nature* **408** 944
- [5] Dietl T, Ohno H, Matsukura F, Cibert J and Ferrand D 2000 *Science* **287** 1019
- [6] Sato K and Katayama-Yoshida H 2001 *Physica B* **308** 904
- [7] Mukherjee D, Dhakal T, Srikanth H, Mukherjee P and Witanachchi S 2010 *Phys. Rev. B* **81** 205202
- [8] Jung S W, An S J, Yi G C, Jung C U, Lee S I and Cho S 2002 *Appl. Phys. Lett.* **80** 4561
- [9] Droubay T C, Keavney D J, Kaspar T C, Heald S M, Wang C M, Johnson C A, Whitaker K M, Gamelin D R and Chambers S A 2009 *Phys. Rev. B* **79** 155203
- [10] Fukumura T, Jin Z, Kawasaki M, Shono T, Hasegawa T, Koshihara S and Koinuma H 2001 *Appl. Phys. Lett.* **78** 958
- [11] Kundaliya D C, Ogale S B, Lofland S E, Dhar S, Metting C J, Shinde S R, Ma Z, Varughese B, Ramanujachary K V, Salamanca-Riba L and Venkatesan T 2004 *Nat. Mater.* **3** 709
- [12] Zheng R K, Liu H, Zhang X X, Roy V A L and Djuricic A B 2004 *Appl. Phys. Lett.* **85** 2589
- [13] Cheng X M and Chien C L 2003 *J. Appl. Phys.* **93** 7876
- [14] Inamdar D Y, Lad A D, Pathak A K, Dubenko I, Ali N and Mahamuni S 2010 *J. Phys. Chem. C* **114** 1451
- [15] Steven D C 2000 *Los Alamos Sci.* **26** 422
- [16] Céspedes E, Laguna-Marco M A, Jiménez-Villacorta F, Chaboy J, Boada R, Guglieri C, Andrés A D and Prieto C 2011 *J. Phys. Chem. C* **115** 24092
- [17] Zhang L, Li J, Du Y, Wang J, Wei X, Zhou J, Cheng J, Chu W, Jiang Z, Huang Y, Yan C, Zhang S and Wu Z 2012 *New J. Phys.* **14** 013033
- [18] Cheng Y, Hao W, Xu H, Yu Y, Wang T, Chen R, Zhang L, Du Y, Wang X L and Dou S X 2012 *ACS Appl. Mater. Interfaces* **4** 4470
- [19] Park C H and Chadi D J 2005 *Phys. Rev. Lett.* **94** 127204
- [20] Hao W, Li J, Xu H, Wang J and Wang T 2010 *ACS Appl. Mater. Interfaces* **2** 2053
- [21] Wang Z H, Geng D Y, Guo S, Hu W J and Zhang Z D 2008 *Appl. Phys. Lett.* **92** 242505
- [22] Manivannan A, Dutta P, Glaspell G and Seehra M S 2006 *J. Appl. Phys.* **99** 08M110
- [23] Sharma V K and Varma G D 2007 *J. Appl. Phys.* **102** 056105
- [24] Segura-Ruiz J, Martínez-Criado G, Chu M, Geburt S and Ronning C 2011 *Nano Lett.* **11** 5322
- [25] Kohler T, Armbruster T and Libowitzky E 1997 *J. Solid State Chem.* **133** 486
- [26] Du C L, Gu Z B, Lu M H, Wang J, Zhang S T, Zhao J, Cheng G X, Heng H and Chen Y F 2006 *J. Appl. Phys.* **99** 123515
- [27] Bundesmann C, Ashkenov N, Schubert M, Spemann D, Butz T, Kaidashev E M, Lorenz M and Grundmann M 2003 *Appl. Phys. Lett.* **83** 1974
- [28] Alaria J, Bouloudenine M, Schmerber G, Colis S, Dinia A, Turek P and Bernard M 2006 *J. Appl. Phys.* **99** 08M118
- [29] Samanta K, Dussan S, Katiyar R S and Bhattacharya P 2007 *Appl. Phys. Lett.* **90** 261903
- [30] Cong C J, Liao L, Liu Q Y, Li J C and Zhang K L 2006 *Nanotechnology* **17** 1520
- [31] Han Y F, Ramesh K, Chen L, Widjaja E, Chilukoti S and Chen F 2007 *J. Phys. Chem. C* **111** 2830
- [32] Hu C C, Wu Y T and Chang K H 2008 *Chem. Mater.* **20** 2890
- [33] Chen Y, Hao W C, Li W X, Xu H Z, Chen R and Dou S X 2013 *Chin. Phys. B* **22** 107501
- [34] Nogués J, Sort J, Langlais V, Skumryev V, Suriñach S, Muñoz J S and Baró M D 2005 *Phys. Rep.* **422** 65
- [35] West K, Nam D, Lu J, Bassim N, Picard Y, Stroud R and Wolf S 2010 *J. Appl. Phys.* **107** 113915
- [36] Sun Y, Cong J Z, Chai Y S, Yan L Q, Zhao Y L, Wang S G, Ning W and Zhang Y H 2013 *Appl. Phys. Lett.* **102** 172406
- [37] Martínez B, Sandiumenge F, Balcels L, Arbiol J, Sibieude F and Monty C 2005 *Phys. Rev. B* **72** 165202
- [38] Nagamiya T, Yosida K and Kubo R 1955 *Adv. Phys.* **4** 1
- [39] Park J K, Lee K W, Kweon H and Lee C E 2011 *Appl. Phys. Lett.* **98** 102502